

ISSI Visiting Scientists Programme

THE RHESSI MISSION: X-RAY SPECTRA AND IMAGE ANALYSIS BY MEANS OF INVERSION METHODS.

Team Leader: Anna Maria Massone
(CNR-INFN LAMIA, Genova, Italy)

Report of the First Group Meeting:
September 22-28, 2005

Spectroscopy

Electron-electron bremsstrahlung emission

X-ray emission from solar flares is a combination of the electron-proton and electron-electron bremsstrahlung. Electron-electron bremsstrahlung becomes significant at electron and photon energies above 300 keV.

The cross-section Q for bremsstrahlung is in general equal to

$$Q = Z^2 Q_{e-p} + Z Q_{e-e} \quad (1)$$

where Z is the average atomic number in the plasma, Q_{e-p} is the cross-section for bremsstrahlung production in electron-proton collisions [6] and Q_{e-e} is the cross-section for electron electron bremsstrahlung [3].

During this meeting, we included the electron-electron bremsstrahlung in the inversion routine package and we studied its influence at energies higher than 300 keV on the inferred mean electron spectra for a given hard X-ray spectrum - Fig. 1(a) - coming from the January 17, 2005 flare (09:43:16 - 09:44:24 UT).

As shown in Fig. 1(b), the inclusion of electron-electron bremsstrahlung makes the electron spectrum required to produce the given hard X-ray spectrum steeper at high energies. The electron spectrum with e-e bremsstrahlung included is nearly a single power law, while the other flattens.

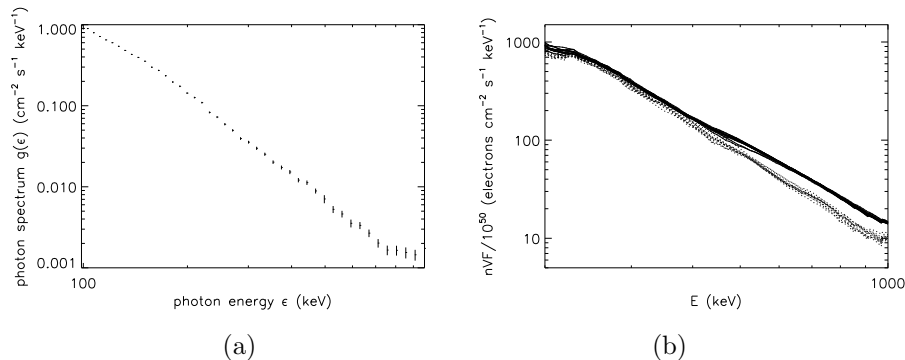


Figure 1: (a) Input photon spectrum. (b) Regularized electron spectra with the e-p bremsstrahlung contribution (solid lines) and with the inclusion of e-e bremsstrahlung (dotted lines).

Blind tests and resolution

The relation between the measured photon spectrum $g(\epsilon)$ and the mean electron flux spectrum $\bar{f}(E)$ is described by a Volterra integral equation of the first kind [1]:

$$g(\epsilon) = \int_{\epsilon}^{\infty} \bar{f}(E)Q(\epsilon, E)dE \quad (2)$$

We considered a systematic comparison of the effectiveness of three different approaches for the inversion of Eq. 2 (Parametric forward-fitting [4], Matrix inversion with data-adaptive binning [5], Tikhonov regularization theory [8]). We have performed such comparison by means of *blind* tests, whereby physically significant synthetic photon spectra have been inverted without knowing $\bar{f}(E)$ in advance.

During the meeting we discussed final issues about the paper *Evaluation of Algorithms for Reconstructing Electron Spectra from their Bremsstrahlung Hard X-Ray Spectra*. In particular considerations about the resolution problem led to the inclusion of an Appendix in the paper, which has been submitted to *The Astrophysical Journal*.

Flares with post-albedo correction spectral flattening

During the meeting we discussed the problem of flare spectra which show flattening after isotropic albedo correction. The analysis of

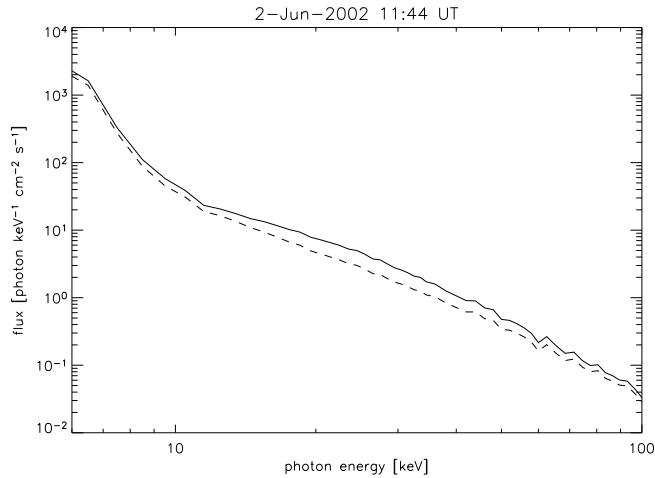


Figure 2: Hard X-ray spectrum of the 2 Jun 2002 flare. The full line corresponds to the total spectrum (with albedo contribution), the dashed is the photon spectrum corrected for albedo in the isotropic approximation.

RHESSI flare spectra recently confirmed that the contribution of flare primary photons back-scattered by the photosphere (albedo) can cause flattening of observed photon spectra below around 30 keV and modify the corresponding electron flux spectra. The albedo can introduce a spectral feature in electron spectra that can be interpreted as a low-energy cutoff of the beam electron flux distribution. The existence and the value of the low-energy cutoff plays an important role in the evaluation of the energetics of the electron beams.

Moreover, several examples of flare photon spectra have been studied which still show flattening after the contribution of albedo in the isotropic approximation was removed. Some of these flares are now being analysed also by J. Kašparová and E. Kontar who concentrate on albedo signatures in flare spectra with respect to their spatial distribution on the solar disk. We discussed together several possible effects which could cause the flattening:

1. existence of the low-energy cutoff inherent to the electron beams, i.e. not as an artefact due to the albedo contribution. Such a low-energy cutoff can be alternatively defined as a power-law index δ of forward-fitted injected electron flux distribution F_0 . If $\delta \leq 2$, then the energy flux of the beam is finite without introducing a sharp low-energy cutoff.

2. anisotropy of the primary source which results in underestimation of the albedo correction (i. e. using isotropic approximation).

An example of a photon spectrum which seems to be consistent with a low-energy cutoff in F_0 after the isotropic albedo correction is shown in Fig. 2.

Imaging Spectroscopy

The RHESSI mission combines, for the first time, high-resolution imaging in hard X-rays and gamma rays with high-resolution spectroscopy, so that a detailed energy spectrum can be obtained at each point of the image.

Such *imaging spectroscopy* [2, 7] allows spectral changes to be measured as the electrons propagate along the magnetic field in the flaring loop or loops. It represents an important new capability not previously available in this wavelength range that will provide powerful new constraints on the mechanisms of energy gain and loss.

During the meeting we performed investigations in this direction. We selected the April 15, 2002 (00:01:20 - 00:02:20 UT) flare and we built ten images of the flare corresponding to different X-ray energy bands (Fig. 3) by using the CLEAN algorithm.

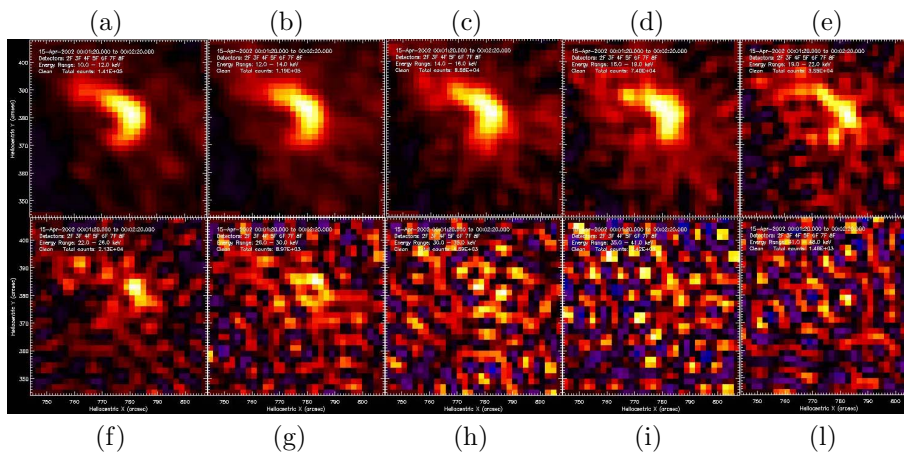


Figure 3: Images of the selected flare in the X-ray energy bands : a) 10-12 keV; b) 12-14 keV; c) 14-16 keV; d) 16-19 keV; e) 19-22 keV; f) 22-26 keV; g) 26-30 keV; h) 30-35 keV; i) 35-41 keV; l) 41-48 keV.

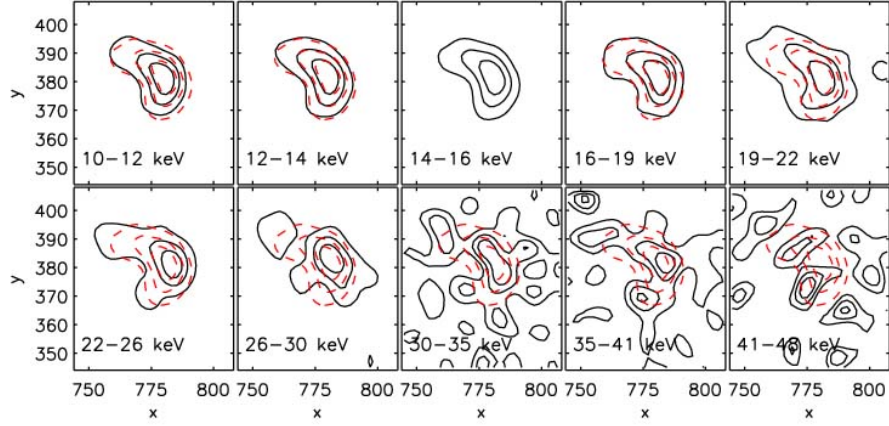


Figure 4: Isocontours corresponding to 25%, 50% and 75% of each maximum. Red curves are the isocontours of panel 3.

Selecting the isocontours corresponding to 25%, 50% and 75% of the maximum in each image we obtain the plots of Fig. 4, where the isocontours of panel 3 (14 – 16 keV) are drawn together with the others for reference.

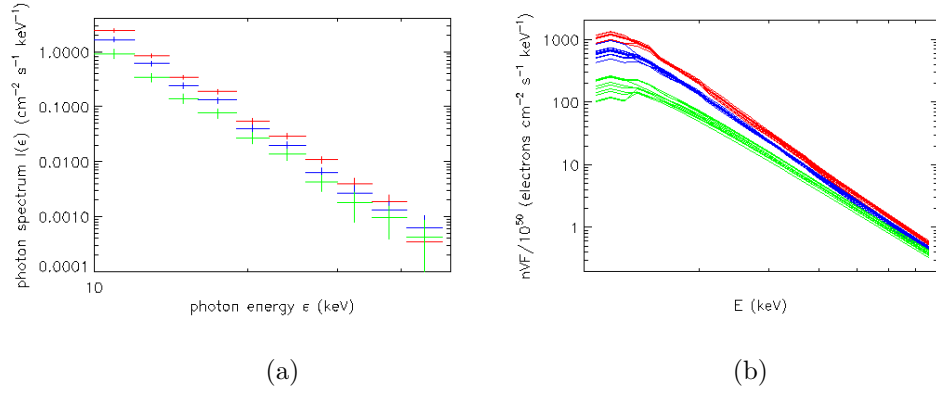


Figure 5: (a) Photon spectra corresponding to the flux in the inner (red), central (blue) and outer region (green). (b) Reconstructed electron spectra.

The isocontours of panel 3 divide each panel in three different regions (+ background) for which we can calculate the corresponding total photon flux as the sum of the values of the pixels that are inside each region. In this way we obtain three photon spectra carrying

information on the activity in the center and in the boundaries of the loop - Fig. 5(a) -. Fig. 5(b) shows that the reconstructed electron spectra are clearly distinguishable.

A different choice of the regions (North, Middle and South as in Fig. 6) leads to photon spectra - Fig. 7(a) - and consequently to reconstructed electron spectra - Fig. 7(b) - with more similar shape. In particular the electron spectra corresponding to the North and South regions seem to overlap, suggesting an interesting symmetry in those regions of the loop. In other words, the legs of the loop have about the same spectrum, and the spectrum at the looptop (Middle) is steeper than that of the legs (N & S).

As a further test, we compared the photon spectrum obtained from all pixels in all panels and the one coming from spectroscopy. In Fig. 8(a) the two spectra are superimposed while in Fig. 8(b) the corresponding reconstructed electron spectra are represented. We agreed that the differences in the photon spectra, and the origin and nature of the dip in the electron spectrum from the images are open issues for future analysis.

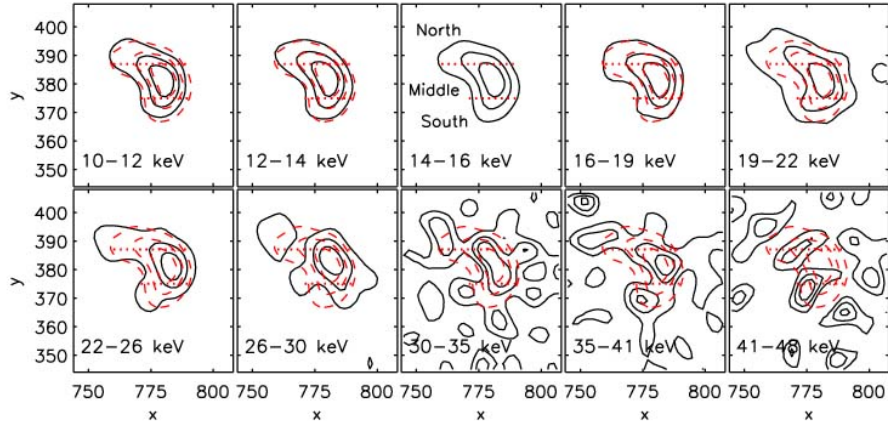


Figure 6: North: region between the 25% isocontour and the upper dotted line; Middle: region between the 25% isocontour and the two dotted lines; South: region between the 25% isocontour and the lower dotted line. Red curves are the isocontours of panel 3.

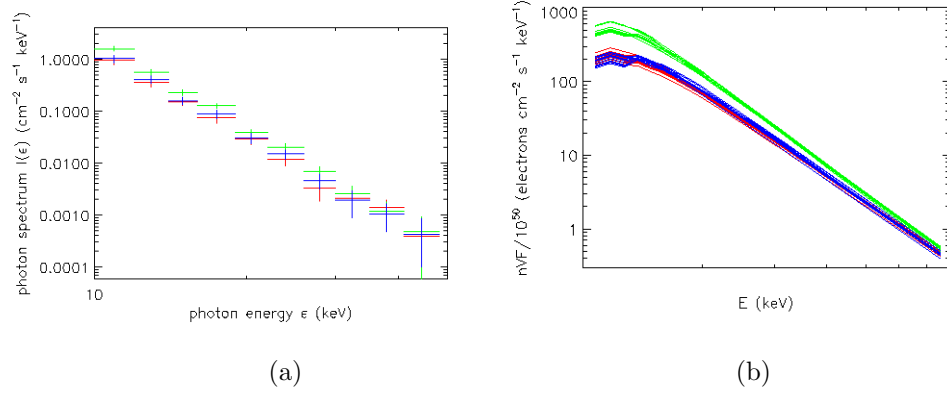


Figure 7: (a) Photon spectra corresponding to the flux in the North (red), South (blue) and Middle region (green). (b) Reconstructed electron spectra.

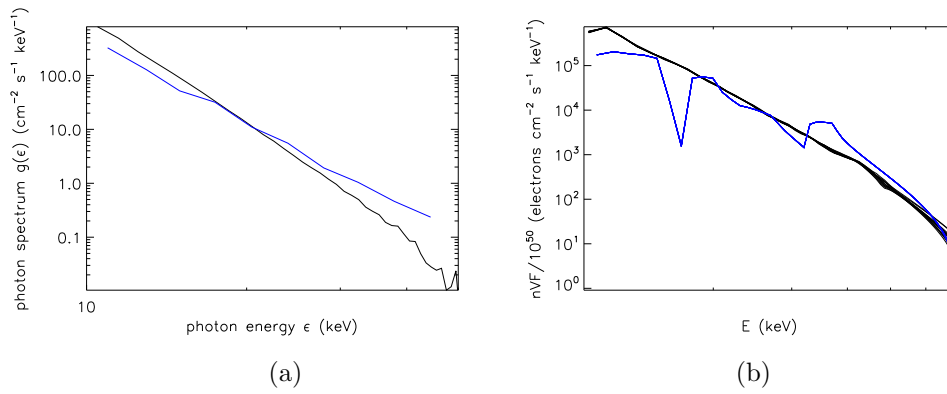


Figure 8: (a) Integrated photon spectra from spectroscopy (black) and from imaging-spectroscopy (blue); (b) the corresponding reconstructed electron spectra.

Bibliography

- [1] Brown J.C., Emslie A.G. and Kontar E.P., 2003, ApJ, **595**, L115.
- [2] Emslie et al. 2003, ApJ, **595**, L107.
- [3] Haug, E., 1998, Solar Phys., **178**, 341.
- [4] Holman GD, Sui L, Schwartz RA, and Emslie AG, 2003, ApJ, **595**, L97.
- [5] Johns, C.M. and Lin, R.P., 1992, Solar Physics, **137**, 121.
- [6] Koch, H.W., & Motz J.W., 1959, Phys. Rev., **31**, 920.
- [7] Sui et al. 2002, Solar Physics, **210**, 245.
- [8] Tikhonov A.N., 1963, Dokl. Akad. Nauk., USSR, **153**, 501-504.